UC Merced

UC Merced Previously Published Works

Title

Ultrafast folding kinetics of WW domains reveal how the amino acid sequence determines the speed limit to protein folding.

Permalink

https://escholarship.org/uc/item/5sk8p2pd

Journal

Proceedings of the National Academy of Sciences of USA, 116(17)

Authors

Szczepaniak, Malwina
Iglesias-Bexiga, Manuel
Cerminara, Michele
et al.

Publication Date

2019-04-23

DOI

10.1073/pnas.1900203116

Peer reviewed

eScholarship.org Powered by the California Digital Library
University of California

Ultrafast folding kinetics of WW domains reveal how the amino acid sequence determines the speed limit to protein folding

Malwina Szczepaniak[a], Manuel Iglesias-Bexiga[b], Michele Cerminara[a,c], Mourad Sadqi[c,d,e], Celia Sanchez de Medina[a,c], Jose C. Martinez[b], Irene Luque[b], and Victor Muñoz[a,c,d,e,f,1]

[a]Centro de Investigaciones Biológicas, Consejo Superior de Investigaciones Científicas, 28040 Madrid, Spain; [b]Departamento de Química Física e Instituto de Biotecnología, Facultad de Ciencias, Universidad de Granada, 18071 Granada, Spain; [c]Centro Nacional de Biotecnología, Consejo Superior de Investigaciones Científicas, Campus de Cantoblanco, 28049 Madrid, Spain; [d]Department of Bioengineering, School of Engineering, University of California, Merced, CA 95343; [e]Center for Cellular and Biomolecular Machines, University of California, Merced, CA 95343; and [f]Nanobiosystems Programme, Instituto Madrileño de Estudios Avanzados Nanociencia, 28049 Madrid, Spain

Edited by Martin Gruebele, University of Illinois at Urbana–Champaign, Urbana, IL, and approved March 19, 2019 (received for review January 5, 2019)

Protein (un)folding rates depend on the free-energy barrier separating the native and unfolded states and a prefactor term, which sets the timescale for crossing such barrier or folding speed limit. Because extricating these two factors is usually unfeasible, it has been common to assume a constant prefactor and assign all rate variability to the barrier. However, theory and simulations postulate a protein-specific prefactor that contains key mechanistic information. Here, we exploit the special properties of fast-folding proteins to experimentally resolve the folding rate prefactor and investigate how much it varies among structural homologs. We measure the ultrafast (un)folding kinetics of five natural WW domains using nanosecond laser-induced temperature jumps. All five WW domains fold in microseconds, but with a 10-fold difference between fastest and slowest. Interestingly, they all produce biphasic kinetics in which the slower phase corresponds to reequilibration over the small barrier (<3 *RT*) and the faster phase to the downhill relaxation of the minor population residing at the barrier top [transition state ensemble (TSE)]. The fast rate recapitulates the 10-fold range, demonstrating that the folding speed limit of even the simplest all-β fold strongly depends on the amino acid sequence. Given this fold's simplicity, the most plausible source for such prefactor differences is the presence of nonnative interactions that stabilize the TSE but need to break up before folding resumes. Our results confirm long-standing theoretical predictions and bring into focus the rate prefactor as an essential element for understanding the mechanisms of folding.

protein folding | rate theory | rate prefactor | folding mechanisms | free-energy barrier

In their natural environment, proteins fluctuate stochastically between their marginally stable folded 3D structure and a disordered ensemble with rates that determine their biological properties. These rates, which hold the key to the underlying folding mechanisms, vary vastly, resulting in folding and unfolding times that range from a few microseconds to months (1). Such enormous variability highlights the underlying mechanistic complexity of a process that involves collective motions around thousands of protein and solvent coordinates, and formation and dissolution of cooperative networks of weak interactions (2). Theory describes protein (un) folding rates as diffusion on a free-energy surface obtained by projecting the protein–solvent hyperdimensional phase space (or folding energy landscape) onto one or few order parameters that capture the reaction's progress (3–5). Because projected folding free-energy surfaces (FESs) tend to show two metastable wells (native and unfolded) (6, 7), such description often reduces to Kramers rate theory (8), which defines the rate of escape from each well as follows:

$$k = \frac{\beta D \omega \omega^*}{2\pi} \exp(\beta \Delta G^*), \qquad [1]$$

where D is the diffusion coefficient at the top of the barrier separating the two wells, ω^2 is the curvature of the well (folded or unfolded), $-(\omega^*)^2$ is the curvature at the barrier top, $\beta = 1/k_B T$ (where k_B is the Boltzmann constant and T is the temperature), and ΔG^* is the height of the free-energy barrier. Here, it is important to note that D is not the Stokes–Einstein translational diffusion coefficient, but an effective term that depends on many factors, including the conformational motions responsible for crossing the barrier (9), the kinetic connections between conformations within the transition state ensemble (TSE) (10), and the energetic roughness of the folding landscape (11). The rate thus depends exponentially on the barrier height whereas the preexponential term (or prefactor) defines the timescale for crossing over the barrier (8).

One key issue in using Eq. **1** is that its two terms cannot be extricated from the rates measured experimentally. Accordingly, common practice has been to assume a constant prefactor or folding speed limit (12), and focus on the barriers as differential factor given their exponential rate dependence (13). In early times, it was not even clear what the right magnitude might be for such folding rate prefactor. More recently, extensive biophysical work has converged onto an estimate of ∼1/(1 μs) (14). This timescale is consistent with multivariate approaches, including measurements of elementary folding motions (15), extrapolations from size scaling of folding rates (16), or the timescales of the fastest folding (17) and one-state downhill folding (18) proteins. Access to empirical estimates of the folding speed limit enabled the

Significance

Natural proteins fold and unfold with rates that define their biological properties and vary vastly from protein to protein. A major fundamental question refers to how fast a protein can possibly fold, how does this limit compare with chemical reaction rates, and whether it is universal or depends on the protein's chemical properties. We apply ultrafast kinetic methods to investigate five proteins that share the simplest all-β fold but have different amino acid sequence. In these studies, we measure the folding speed limit for each one of them and discover rather substantial differences. Our results shed light onto the fundamentals of biomolecular rate theory and onto our general understanding of how proteins fold, function, and evolve.

Author contributions: V.M. designed research; M. Szczepaniak, M.C., and C.S.d.M. performed research; M.I.-B., J.C.M., and I.L. contributed new reagents/analytic tools; M. Szczepaniak, M.C., M. Sadqi, and V.M. analyzed data; and M. Szczepaniak and V.M. wrote the paper.

The authors declare no conflict of interest.

This article is a PNAS Direct Submission.

Published under the PNAS license.

[1]To whom correspondence should be addressed. Email: vmunoz3@ucmerced.edu.

This article contains supporting information online at www.pnas.org/lookup/suppl/doi:10.1073/pnas.1900203116/-/DCSupplemental.

Published online April 9, 2019.

conversion of rates onto barriers (19), which confirmed key theoretical predictions such as their entropic origin and relatively low heights (i.e., <10 k_BT) (7). In parallel, massive efforts to characterize folding TSEs using mutational analysis have unveiled a strikingly simple rule by which the barrier recapitulates approximately one-third of the total native stabilization free energy, regardless of the protein's structure and sequence, or the position and type of mutation (20). Relative folding and unfolding rates can be in fact predicted reasonably well from protein size alone (16), or significantly better by just adding their structural class assignment (whether the protein is α, β, or mixed) (1).

Those findings hint that the complex folding mechanisms predicted by theory (21) and observed in computer simulations (22) must be subsumed to some degree into the rate prefactor, which should accordingly vary characteristically from protein to protein. Scaling analysis of folding rates points to protein-specific folding prefactors, especially for β-sheet proteins (23). The experimental analysis of the folding prefactor is, however, challenging. One possibility comes from single-molecule methods, which can, in principle, capture the statistically rare barrier crossing events [or transition paths (TPs)] undergone by proteins fluctuating between the native and unfolded states. Such folding TPs have been recently detected using single-molecule fluorescence (24), optical tweezers (25), and atomic force microscopy (26). The somewhat limited experimental information about folding TPs obtained thus far points to a universal rate prefactor (27), with proteins designed de novo and thus not optimized by natural selection as possible exceptions (28). Here, we aim to investigate to what extent the folding rate prefactor, or speed limit, varies among naturally evolved amino acid sequences that fold onto the same native 3D structure. Our rationale is that comparison among structural homologs should unveil the natural variability in folding mechanisms that coexists within a given structural fold. To probe the rate prefactor experimentally, we resource to an alternative kinetic approach that is specific to fast-folding proteins, and that was pioneered by Gruebele and coworkers (29, 30). This kinetic approach relies on probing the downhill relaxation from the barrier top (TSE) on proteins that have marginal folding barriers, and thus detectable TSE populations, using ultrafast kinetic methods. As model proteins, we use a collection of WW domains, which share the simplest antiparallel β-sheet topology found in nature and fold in the microsecond timescale (31–34), and also exhibit the marginally cooperative unfolding thermodynamics of the downhill folding scenario (35).

Results and Discussion

Probing the Folding Prefactor by Experiment. The folding prefactor has been derived from experiments on individual molecules by comparing the characteristic dwell times in the native or the unfolded states (τ_{act}) with the mean TP time (τ_{TP}) (24). There is an alternative approach based on the ultrafast kinetic analysis of fast folders (29). Microsecond folding proteins cross free-energy barriers of height comparable to thermal energy (i.e., <3 *RT*) (36). These shallow barriers result on minor, but significant, TSE populations that must reequilibrate in response to perturbations. The downhill relaxation from the TSE can be detected kinetically provided the method is sufficiently fast (e.g., after a nanosecond temperature jump) (Fig. 1), producing biphasic relaxation kinetics. The fast phase [or "molecular phase" (29)] corresponds to the downhill relaxation of molecules residing in the TSE and follows an expression equivalent to the relaxation on a harmonic well (37) with $(\omega^*)^2$ representing the inverted curvature at the barrier top:

$$k_{mol} = \beta D(\omega^*)^2. \quad [2]$$

Assuming similar curvatures for barrier and well, as done before for the analysis of folding TPs (24), the ratio between the molecular rate and the relaxation rate (the slower kinetic phase from the same experiment) measured at the denaturation midpoint becomes the following:

$$k_{mol}/k_{rel} \approx \pi \exp(-\beta \Delta G^*), \quad [3]$$

where k_{rel} is equal to the right term in Eq. **1** multiplied by 2 (sum of the equal folding and unfolding rates at the midpoint). Eq. **3** directly leads to the free-energy barrier. The rate prefactor is then obtained from the molecular phase as $k_{mol}/2\pi$ (combining Eqs. **2** and **1**). These expressions permit to estimate the barrier and rate prefactor from nanosecond laser-induced temperature jump measurements on fast-folding proteins that exhibit a molecular phase.

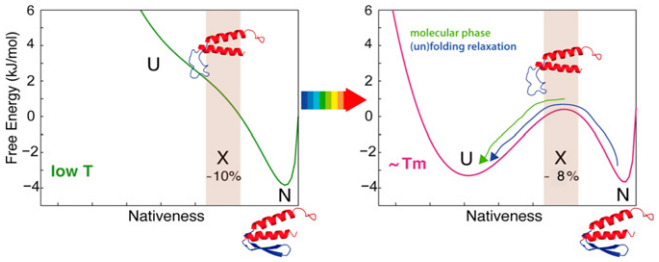

Fig. 1. Measuring folding rate prefactors via ultrafast kinetic experiments. The scheme depicts, as an example, the fast folder gpW and its folding free-energy landscape (50). The *Left* panel shows native conditions (below the T_m) in which the landscape is tilted to the folded state and downhill. The *Right* panel shows the landscape at the midpoint temperature (T_m), which results on the emergence of a small (<2 *RT*) free-energy barrier. The subensemble that corresponds to the barrier top (TSE) at T_m is shown as a gray swath with populations of 10% at low *T* and ~8% at T_m. In response to a nanosecond laser-induced *T* jump that brings the protein to the folding midpoint (rainbow arrow), the excess TSE population quickly reequilibrates on a downhill relaxation toward the unfolded well, or molecular phase (green). The excess native population reequilibrates with the unfolded well more slowly by a relaxation that involves crossing the barrier (blue).

The Range of Folding Rates of Natural WW Domains. WW domains have been very popular models for fast-folding experiments (31–34) and molecular simulations (22, 34, 38) because they are the smallest and fastest natural β proteins. Relative to the fastest α-helical proteins, the natural WW domains studied so far fold moderately fast (near 100 μs) (39). Despite their comparatively slower rates, WW domains tend to fold within the downhill scenario (barriers <3 *RT*) (40) and can exhibit a molecular phase (33). Consistency with the downhill scenario implies an (un)folding rate prefactor that is slower for β than for helical proteins, as it has been proposed theoretically (23). Nevertheless, mutants of the FiP35 WW domain fold somewhat faster (30), and a variant optimized for speed by computational design folds in just 4 μs (34). Here, we measure the ultrafast folding kinetics of five WW domains, including three examples from group I (Nedd4-WW4, Nedd4-WW3, and the L30K mutant of Yap65-WW1) and two from group II (Fbp11-WW1 and Fbp11-WW2) (35). The five domains have marked differences in sequence (~30% homology), but share size and fold topology (*SI Appendix*, Fig. S1). A detailed thermodynamic analysis of these domains has recently demonstrated their minimal cooperativity and downhill-like unfolding thermodynamics (35).

We performed kinetic experiments using an infrared (IR) laser *T*-jump instrument to probe secondary structure from changes in the amide I band absorption within the 1,630–1,640 cm^{-1} range in response to <10-ns temperature jumps of about 10 K (*SI Appendix*). These experiments produced microsecond relaxation decays for all WW domains (Fig. 2*A*). With times starting at 1 μs (the IR detector has 600-ns response time), the measured IR decays can be fit reasonably well to a single-exponential function (Fig. 2*A*). The single-exponential fits render relaxation rates at the midpoint temperature ranging from 1/(55 μs) for Nedd4-WW4 to 1/(10 μs)

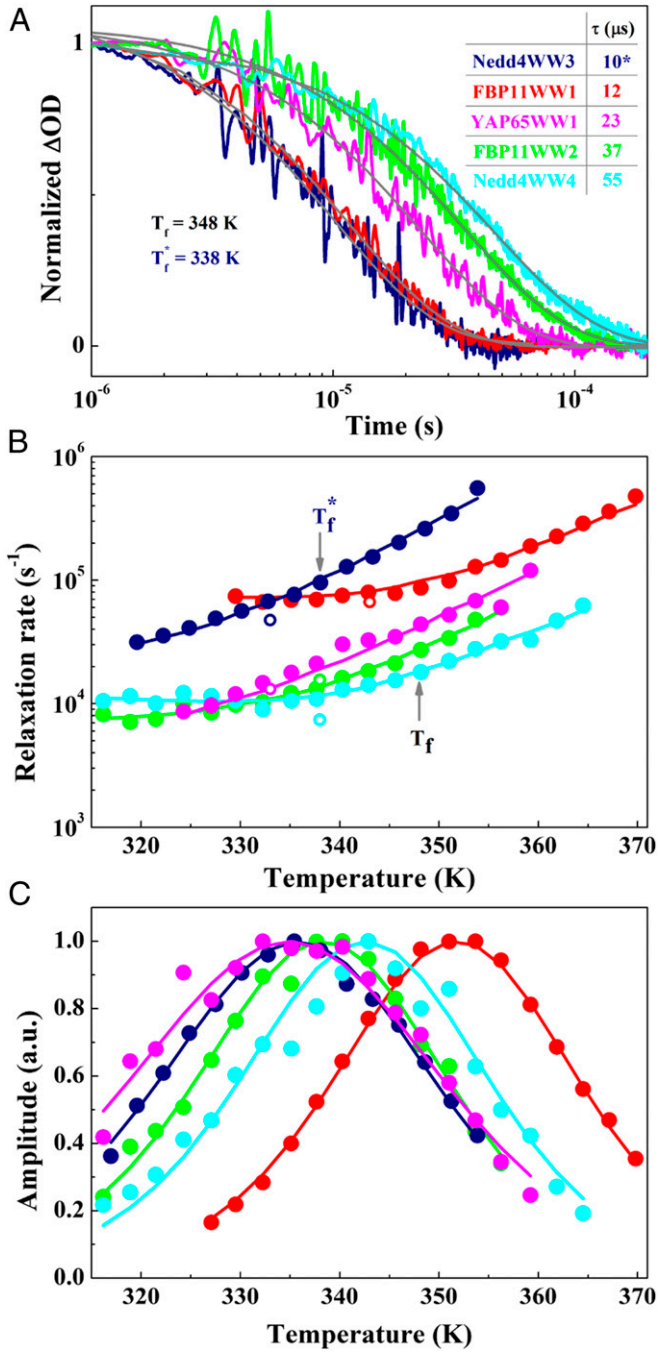

Fig. 2. Range of folding rates on a catalog of WW domains. Ultrafast folding kinetics of the five WW domains measured by the IR laser-induced *T*-jump technique. (*A*) Relaxation decay of the IR absorption at 1,640 cm^{-1} (amide I band) for the five proteins in response to nanosecond *T* jumps of ∼10 K to a final folding temperature of reference (i.e., T_f ∼348 K for all but Nedd4-WW3, which was measured at T_f* ∼338 K due to its lower thermal stability). The color code is provided in the *Inset* of *A*, and as in Fig. S1. Fits to single-exponential functions are shown as gray lines. (*B*) Relaxation rate as a function of temperature for the five WW domains. (*C*) Relative amplitude of the IR signal after *T* jumps of ∼10 K to the final temperatures shown in the abscissa. The maximum in this plot indicates the T_m (maximal amplitude change). The curves in *B* and *C* correspond to the fits to the 1D-FES model only using the data shown as filled circles to minimize biases in the temperature dependence of the rate derived from the analysis (*SI Appendix*, Fig. S1 and Table S1).

for Nedd4-WW3. There are, however, signs of a faster, not well-resolved process in some experimental traces of the slowest folders (see below). The overall relaxation rate for each protein is only weakly temperature dependent, but the total spread in rates is large, ranging from 1/(130 μs) for FBP11-WW2 at the lowest temperatures to 1/(1.5 μs) for Nedd4-WW3 and FBP11-WW1 at the highest probed temperature (Fig. 2*B*). The weakly temperature-dependent global (un)folding rates suggest that folding involves crossing marginal free-energy barriers (<3 *RT*) (40). It is noteworthy that these five natural proteins cover the entire range of (un)folding times previously observed for WW domains. In this regard, the folding relaxation of Nedd4-WW3 (Fig. 3, dark blue) is comparable to that of the record holding, computationally designed FiP35 variant [i.e., 1/(4 μs) at 363 K (34)]. We can thus conclude that our protein catalog spans the rate variability found within the WW fold, including natural and engineered variants.

WW Domains Fold–Unfold Over Marginal Free-Energy Barriers. The spread in rates of Fig. 3 suggests differences in the folding free-energy barrier of up to 2.3 *RT* from fastest to slowest. However, the temperature dependence of the relaxation rate is flat for all domains, as expected for downhill folders (40). To explore this issue in more depth we analyzed the IR kinetic data within a 1- to 200-μs window using a 1D-FES model of protein folding (40, 41). In this model, folding thermodynamics are described using a projection of the energy landscape onto a single local order parameter: nativeness. The kinetic relaxation is described as diffusion over that surface, that is, in Kramers-like fashion. The combination of relaxation rates (Fig. 2*B*) and kinetic amplitudes (Fig. 2*C*) as a function of temperature provides all of the information required to determine the four parameters of the model (*SI Appendix*). This simple kinetic analysis fits the IR experimental data for the five proteins remarkably well (Fig. 2 *B* and *C* and *SI Appendix*, Table S1 for parameters). Interestingly, the 1D-FESs arising from the fitted model are similar for the five domains and feature very small free-energy barriers (∼1 *RT*; *SI Appendix*, Fig. S2). Therefore, the 1D-FES kinetic analysis suggests that the nearly 10-fold rate variation among WW domains does not result from different barriers, but rather from changes in rate prefactor. Large rate differences in structurally homologous proteins have been reported before for spectrin domains, but in that case the rate differences mostly arose from barrier changes (42).

Molecular Phase and Structural Properties of the Folding TSE. To investigate whether these natural WW domains exhibit the molecular phase, we turned to laser *T* jumps using fluorescence detection. Our fluorescence *T*-jump instrument has significantly better time resolution and dynamic range than the IR instrument [10 ns and logarithmic time acquisition (43)], and WW domains have signature fluorescence signal linked to their folding status because their two tryptophan residues engage in specific interactions across the sheet (35). In fluorescence *T*-jump experiments, we indeed detected a time-dependent red shift of the tryptophan emission spectrum (∼5 nm) associated to the unfolding of the five domains. When measured over the entire instrument's dynamic range (10 ns to 2 ms), the kinetic relaxation associated to the spectral shift shows markedly nonexponential decays for all domains that are well fit to a double-exponential function (Fig. 3). A parametric statistical analysis confirms that these decays represent double-exponential rather than single- or stretched-exponential functions (*SI Appendix*, Fig. S3 and Table S2). At the denaturation midpoint, the rates of the slow phase range from 1/(15 μs) to 1/(135 μs). These rates are similar to those measured using IR detection (Fig. 2), but not identical, hinting at the probe-dependent kinetics found in other fast-folding proteins (18). More significantly, an additional much faster phase is observed for all domains with rates ranging from 1/(0.3 μs) to 1/(3 μs) (Fig. 3). The two processes are well separated in time (by a factor of ∼40), and thus both rates are accurately determined from the double-exponential fits (*SI Appendix*, Table S3). The timescales that we obtain for the fast phase are consistent with the molecular phase reported by Gruebele and coworkers on a fast mutant of lambda repressor (29) and

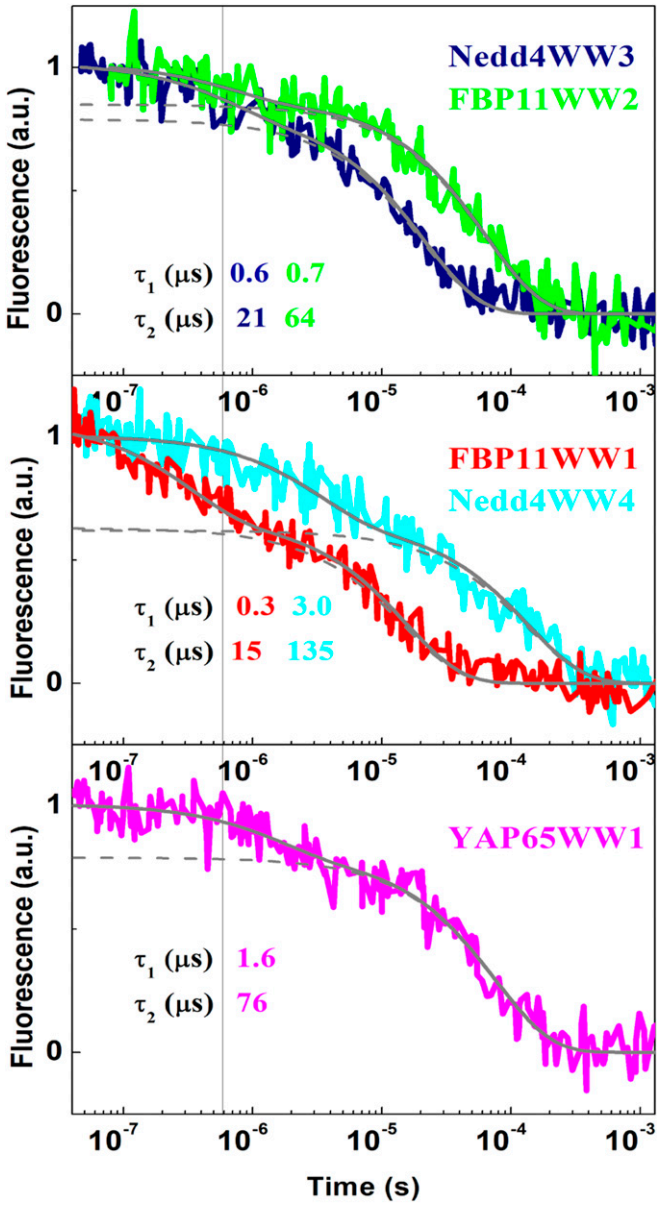

Fig. 3. Biphasic fluorescence *T*-jump kinetics reveal the folding molecular phase or rate prefactor. Ultrafast kinetic decays in logarithmic time monitored by Trp fluorescence in response to ∼10 K nanosecond *T* jumps to final temperature near the mean denaturation midpoint (343 K). The curves are color-coded for each protein as before. The continuous gray curves show the fits of the decays to a double-exponential relaxation, and the dashed curves the fit of the slow phase to a single exponential as reference (extrapolation to zero time of both curves indicate the amplitude of the fast or molecular phase). The relaxation times for the two phases as obtained from the double-exponential fits are shown color-coded in *Insets*.

mutants of other WW domains (33). They are also consistent with the mean folding TP times derived from single-molecule fluorescence experiments on other proteins (27).

These observations agree with the expectation for the molecular phase. However, biexponential folding kinetics with a minor fast phase could also arise from the transient accumulation of a kinetic intermediate separated from the unfolded and native states by free-energy barriers (44). This intermediate can appear on either the native or unfolded sides of the global TSE, corresponding to unfolding or folding kinetic intermediates, respectively. To investigate these possibilities, we built linear three-state kinetic models that represent the two intermediate mechanisms (*SI Appendix*). This modeling exercise indicates that the changes in fast phase amplitude are diagnostic of the folding scenario (*SI Appendix*, Fig. S4). For an unfolding intermediate, the fast-phase amplitude after a typical T jump is minimal up to the denaturation midpoint (T_m), after which point it increases gradually. The opposite is true for a folding intermediate. Our fluorescence *T*-jump experiments show a distinct fast phase around the T_m (Fig. 3) that quickly vanishes at lower and higher temperatures. These results are incompatible with either kinetic intermediate model. In contrast, a maximal fast-phase amplitude at the midpoint is consistent with the changes in population of the barrier top (TSE) for the molecular phase scenario (*SI Appendix*, Fig. S4). The WW-domain fluorescence signal is exquisitely sensitive to minor changes in tertiary environment for the two tryptophans, and thus is likely to be protein specific, consistently with the variation in fast-phase amplitude we see among WW domains (*SI Appendix*, Table S3). In contrast, the IR signal, which reports on overall backbone hydrogen bonding, should be more uniform and likely to change more gradually with temperature. The time resolution of our IR instrument makes it challenging to measure the fast phase detected by fluorescence (Fig. 3, vertical lines at 600 ns), which explains why the IR transients measured from 1 to 200 μs (Fig. 3) are roughly single exponential. Nevertheless, the fluorescence experiments also indicate that the fast phase should be resolvable on the two slowest folders (YAP65-WW1 and Nedd4-WW4) by pushing the IR detection to its 600-ns limit. We could indeed resolve the IR fast phase of these two domains and confirm that its amplitude is maximal at the T_m. Fig. 4 *A*–*C* shows the IR relaxation decays of YAP65-WW1 at three final temperatures, and Fig. 4*D* shows the relative amplitude of the fast phase for the two proteins. Equivalent transients for Nedd4-WW4 are shown in *SI Appendix*, Fig. S5. Parametric statistical analysis confirms that the transients for both proteins are biexponential. The double-exponential fits indicate that the fast-phase amplitude peaks at ∼15–20% near the T_m and drops to ∼10% at 10° below or above (*SI Appendix*, Table S4). In light of these results, we can conclude that the changes in fluorescence (Fig. 3) and IR (Fig. 4) associated to the fast phase reflect the reequilibration of a significantly populated TSE. These signals demonstrate concerted changes in tertiary interactions (fluorescence) and β-sheet backbone hydrogen bonds (IR). We can conclude that TSE conformations of YAP65-WW1 and Nedd4-WW4 have partly disrupted β-sheet structure and nonnative packing of the two tryptophan residues. The TSEs of the three faster domains share the tryptophan environment signature as judged by fluorescence (with amplitude differences likely reflecting specific changes in local environment), but we could not obtain information about hydrogen-bonding status since their molecular phase is too fast for IR detection.

Variability in Folding Rate Prefactor Within the WW Fold. The kinetic data of Fig. 3 reveal a strong correlation between the rates of the fast and slow phases for these WW domains (r = 0.91 with a slope of 1 in a log–log correlation; Fig. 5). Such correlation demonstrates that the differences in (un)folding rates propagate almost exactly to the fast phase rates, consistently with the molecular phase (see below), and not with the accumulation of an intermediate. The intercept with the ordinate in this plot indicates an average ratio between the fast phase (k_{mol}) and slow phase (k_{rel}) of 40. Using Eq. **3**, a 40-fold ratio converts onto an estimated mean (un)folding barrier of 2.5 *RT* for the WW fold. A mean barrier of 2.5 *RT* further confirms the classification of these proteins as incipient downhill folders, but it is moderately higher than the barriers estimated from the 1D-FES kinetic analysis (about 1 *RT*). The level of consistency between kinetic barrier estimates is nevertheless remarkable given the different assumptions made on each procedure. For instance, the curvature of the ground states and (inverted) barrier are assumed equal in the rate ratio procedure (Eq. **3**), but the 1D-FESs have different curvatures (*SI Appendix*, Fig. S2). Likewise, how the prefactor's temperature dependence is introduced into the model affects the magnitude of the barrier obtained from the temperature

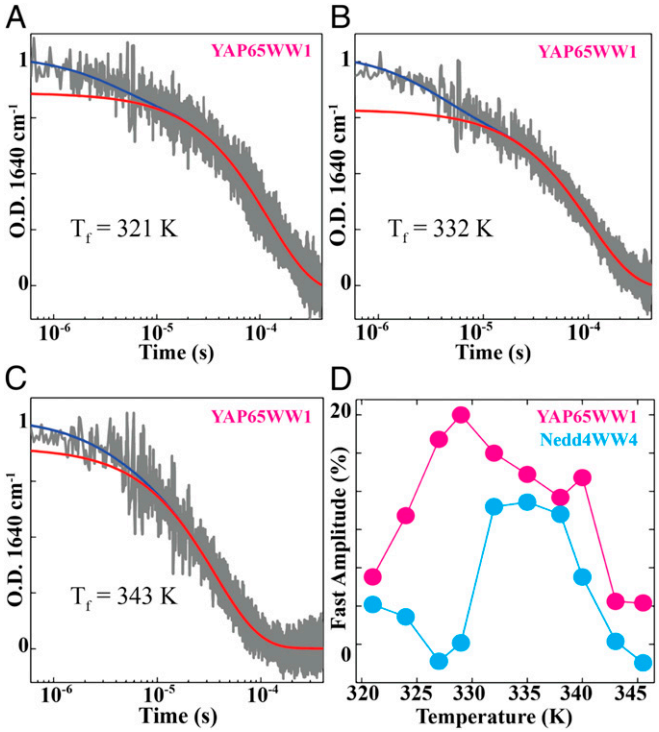

Fig. 4. The amplitude of the molecular phase is maximal at the denaturation midpoint. (*A–C*) Microsecond relaxation IR absorption decays at 1,640 cm^{-1} (amide I band) of YAP65-WW1 in response to ~10 K nanosecond laser *T* jumps to final temperatures of 321, 332, and 343 K. Fits to a double-exponential function are shown in blue, and the single-exponential decay corresponding to the slow phase in red. The difference between the two fits at time 0 reflects the amplitude of the fast phase. (*D*) Relative amplitude for the fast phase determined from IR *T*-jump experiments on YAP65-WW1 (pink) and Nedd4-WW4 (cyan) (*SI Appendix*, Fig. S4). The fitting errors from the double-exponential fits to the transients from both proteins are given in *SI Appendix*, Table S4.

dependence of the rate. Most importantly, given that the prefactor is the only term that affects equally the molecular phase (Eq. **2**) and the activated slow phase (Eq. **1**), Fig. 5 confirms that the rate variability found for these natural WW domains does not come from the barrier, but rather from a sequence-specific folding speed limit. Further confirmation is provided by the fast-phase amplitude, which does not decrease proportionally to the relaxation rate of the domain, as it should be the case if the barrier grows (Fig. 3 and *SI Appendix*, Table S3). We can thus derive the rate prefactor for each individual protein by simply dividing their molecular rate by 2π (see above). This calculation produces speed limits that range from as fast as 1/(2 μs) for FBP11-WW1 (Fig. 3, red) to as slow as 1/(19 μs) for Nedd4-WW4 (Fig. 4, cyan). That is, we find that the rate prefactor for a set of fast-folding proteins that share size and native fold varies by at least a factor of 10.

Conclusions

We show that the five WW domains of this study are fast folders (Figs. 2 and 3). A previous in-depth thermodynamic analysis of these domains showed that their equilibrium unfolding is minimally cooperative and characteristic of downhill folding (35). Using two independent kinetic procedures, we find that the five WW domains cross a small folding free-energy barrier at the denaturation midpoint. The kinetic barrier is comparable to thermal energy (<3 *RT*), confirming that these β-proteins fold within the downhill scenario but are not one-state folders. Similar analyses on α-helical (45) and mixed α+β (46) fast-folders have also produced slightly higher kinetic than thermodynamic barriers. Consistently lower thermodynamic barriers suggest that conformations classified as members of the TSE according to their structural-energetics properties (i.e., by a free-energy projection) may not be directly connected in kinetic microscopic terms. The overall effect is minor, however, as it seems to account for infraestimations of only 1–2 *RT* on the overall folding and unfolding rates.

A second important conclusion refers to the magnitude of the folding prefactor for β-proteins. The folding speed limit that we obtain for the simplest β-fold is 8(±6) μs, which is slower than the speed limit for α-helical and mixed α+β-proteins (14). This average speed limit is, on the other hand, consistent with the mean TP time that Chung and Eaton (27) obtained for a different WW domain using single-molecule FRET. The latter was measured in highly viscous solutions, but both the raw and viscosity corrected data are within the range established by our data. Therefore, β-folds seem to have slower rate prefactors than helix-rich folds. A slower prefactor for beta proteins was anticipated theoretically by Thirumalai and coworkers (23). Here, we confirm this prediction by experiment. One reason behind a slower prefactor for β-folds is likely their need to organize around the β-turns, which results in few productive pathways that are kinetically disconnected from one another, as observed in molecular dynamics (MD) simulations (34). In this scenario, a folding molecule must backtrack to the unfolded state to switch pathways, a subtle kinetic effect that reduces the flux over the barrier resulting in a slower effective diffusion coefficient. In contrast, the folding of α-helical structures starts from many alternative nucleation sites and continues via broadly exchangeable pathways (22, 47).

Finally, we find that the folding speed limit of the simplest antiparallel β-fold varies by at least one order of magnitude among naturally evolved proteins. Such variability is remarkable since it does not stem from structural constraints but from their differences in amino acid sequence (Fig. 2). In this regard, the most likely factor is a significant (and variable) contribution from nonnative interactions to the stabilization of the folding TSE. Nonnative interactions can trap the protein while in transit over the barrier, increasing energy roughness, or internal friction (48), and slowing down the effective intramolecular diffusion coefficient (i.e., smaller prefactor). Off-register electrostatic interactions cause longer TP times on a de novo designed α-helical protein, as was determined using single-molecule FRET experiments and MD simulations (28). Here, however, the differences

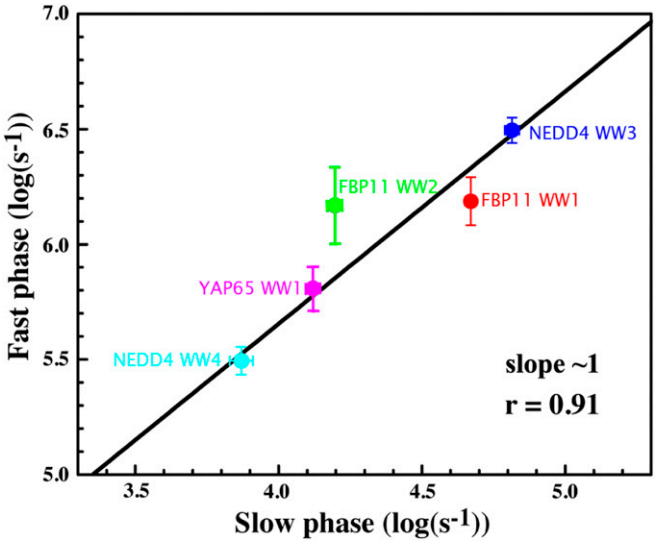

Fig. 5. Molecular versus relaxation rates. Correlation between the relaxation rate (slow phase: from 65,000 to 8,000 s^{-1}) and molecular rate (fast phase: from 3,100,000 to 310,000 s^{-1}) for the five WW domains (color-coded as before) measured near the T_m by the fluorescence *T*-jump method. The rates are shown as base 10 logarithms. The error bars across both axes correspond to the fitting error at 95% confidence from the double-exponential fits (*SI Appendix*, Table S3). The log–log linear correlation produces a slope near 1 and a correlation coefficient *r* of 0.91.

in prefactor are found for natural proteins subjected to similar evolutionary pressure. It thus seem that β-folds are more prone to form nonnative interactions, possibly because slight changes in β-turn position or geometry produce alternative structures stabilized by off-register backbone hydrogen bonds and hydrophobic interactions, an effect that has been reported on de novo designed α-β–miniproteins (49). The differences in prefactor that we observe in just one fold are of the same magnitude as the experimental rate variability that is leftover after correcting for size and structural class effects (1), which provides a simple explanation for the difficulty found to further improve rate predictions. The key implication is that folding rate prefactors contain important mechanistic information that is overlooked in conventional experiments. We should thus measure folding TPs, and/or molecular phases, for a larger catalog of proteins to better understand their fold and sequence determinants, as well as their connection to the underlying mechanisms. Investigating their dependence on solvent viscosity would also help to determine whether the differences in rate prefactor are caused by internal friction (48).

Materials and Methods

An extended description of materials, methods, and procedures is provided in *SI Appendix*. Genes encoding the sequences of FBP11-WW1 and FBP11-WW2, YAP65-WW1, Nedd4-WW3, and Nedd4-WW4 were cloned, and proteins were expressed and purified, as described previously (35). The laser-induced *T*-jump experiments consisted in inducing jumps of ∼10 K with a <10-ns IR pulse and monitoring the protein relaxation by either IR absorption or fluorescence. For IR detection, we monitored the changes in the IR amide I band (at 1,633 cm^{-1} for Nedd4-WW3 and 1,640 cm^{-1} for the other WW domains) and used samples at ∼1 mM concentration in 20 mM phosphate buffer (pH 7). For fluorescence, we measured the tryptophan fluorescence emission spectrum at a sequence of times after the heating pulse on protein samples at 150 μM concentration in 20 mM sodium phosphate buffer (pH 7) containing 2% CS_2 as tryptophan triplet quencher. The relaxation rates and amplitudes obtained from single-exponential fits of the IR *T*-jump experiments were analyzed with a 1D-FES model of protein folding as described previously (46).

ACKNOWLEDGMENTS. This research has been funded by Grant ERC-2012-ADG-323059 from the European Research Council and Grant NSF-MCB-1616759 from the National Science Foundation. V.M. also acknowledges support from the W. M. Keck Foundation and the Center for Cellular and Biomolecular Machines at University of California, Merced (Grant NSF-CREST-1547848). I.L. acknowledges support from the Spanish Ministry of Science and Education through Grants BIO2012-39922-CO2-01 and BIO2016-787746-C2-1-R, and the European Union through Fonds Européen de Développement Économique et Régional.

1. De Sancho D, Muñoz V (2011) Integrated prediction of protein folding and unfolding rates from only size and structural class. *Phys Chem Chem Phys* 13:17030–17043.
2. Brooks CLI, 3rd, Gruebele M, Onuchic JN, Wolynes PG (1998) Chemical physics of protein folding. *Proc Natl Acad Sci USA* 95:11037–11038.
3. Socci ND, Onuchic JN, Wolynes PG (1996) Diffusive dynamics of the reaction coordinate for protein folding funnels. *J Chem Phys* 104:5860–5868.
4. Berezhkovskii A, Szabo A (2005) One-dimensional reaction coordinates for diffusive activated rate processes in many dimensions. *J Chem Phys* 122:14503.
5. Best RB, Hummer G (2011) Diffusion models of protein folding. *Phys Chem Chem Phys* 13:16902–16911.
6. Dinner AR, Sali A, Smith LJ, Dobson CM, Karplus M (2000) Understanding protein folding via free-energy surfaces from theory and experiment. *Trends Biochem Sci* 25:331–339.
7. Portman JJ, Takada S, Wolynes PG (2001) Microscopic theory of protein folding rates. I. Fine structure of the free energy profile and folding routes from a variational approach. *J Chem Phys* 114:5069–5081.
8. Hänggi P, Talkner P, Borkovec M (1990) Reaction-rate theory: Fifty years after Kramers. *Rev Mod Phys* 62:251–341.
9. Best RB, Hummer G (2010) Coordinate-dependent diffusion in protein folding. *Proc Natl Acad Sci USA* 107:1088–1093.
10. Veitshans T, Klimov D, Thirumalai D (1997) Protein folding kinetics: Timescales, pathways and energy landscapes in terms of sequence-dependent properties. *Fold Des* 2:1–22.
11. Chavez LL, Onuchic JN, Clementi C (2004) Quantifying the roughness on the free energy landscape: Entropic bottlenecks and protein folding rates. *J Am Chem Soc* 126:8426–8432.
12. Hagen SJ, Hofrichter J, Szabo A, Eaton WA (1996) Diffusion-limited contact formation in unfolded cytochrome c: Estimating the maximum rate of protein folding. *Proc Natl Acad Sci USA* 93:11615–11617.
13. Muñoz V, Eaton WA (1999) A simple model for calculating the kinetics of protein folding from three-dimensional structures. *Proc Natl Acad Sci USA* 96:11311–11316.
14. Kubelka J, Hofrichter J, Eaton WA (2004) The protein folding "speed limit." *Curr Opin Struct Biol* 14:76–88.
15. Eaton WA, Muñoz V, Thompson PA, Henry ER, Hofrichter J (1998) Kinetics and dynamics of loops, α-helices, β-hairpins, and fast-folding proteins. *Acc Chem Res* 31:745–753.
16. Naganathan AN, Muñoz V (2005) Scaling of folding times with protein size. *J Am Chem Soc* 127:480–481.
17. Cellmer T, Henry ER, Kubelka J, Hofrichter J, Eaton WA (2007) Relaxation rate for an ultrafast folding protein is independent of chemical denaturant concentration. *J Am Chem Soc* 129:14564–14565.
18. Li P, Oliva FY, Naganathan AN, Muñoz V (2009) Dynamics of one-state downhill protein folding. *Proc Natl Acad Sci USA* 106:103–108.
19. Akmal A, Muñoz V (2004) The nature of the free energy barriers to two-state folding. *Proteins* 57:142–152.
20. Naganathan AN, Muñoz V (2010) Insights into protein folding mechanisms from large scale analysis of mutational effects. *Proc Natl Acad Sci USA* 107:8611–8616.
21. Onuchic JN, Luthey-Schulten Z, Wolynes PG (1997) Theory of protein folding: The energy landscape perspective. *Annu Rev Phys Chem* 48:545–600.
22. Lindorff-Larsen K, Piana S, Dror RO, Shaw DE (2011) How fast-folding proteins fold. *Science* 334:517–520.
23. Li MS, Klimov DK, Thirumalai D (2004) Thermal denaturation and folding rates of single domain proteins: Size matters. *Polymer (Guildf)* 45:573–579.
24. Chung HS, McHale K, Louis JM, Eaton WA (2012) Single-molecule fluorescence experiments determine protein folding transition path times. *Science* 335:981–984.
25. Neupane K, et al. (2016) Direct observation of transition paths during the folding of proteins and nucleic acids. *Science* 352:239–242.
26. De Sancho D, Schönfelder J, Best RB, Perez-Jimenez R, Muñoz V (2018) Instrumental effects in the dynamics of an ultrafast folding protein under mechanical force. *J Phys Chem B* 122:11147–11154.
27. Chung HS, Eaton WA (2017) Protein folding transition path times from single molecule FRET. *Curr Opin Struct Biol* 48:30–39.
28. Chung HS, Piana-Agostinetti S, Shaw DE, Eaton WA (2015) Structural origin of slow diffusion in protein folding. *Science* 349:1504–1510.
29. Yang WY, Gruebele M (2003) Folding at the speed limit. *Nature* 423:193–197.
30. Liu F, Nakaema M, Gruebele M (2009) The transition state transit time of WW domain folding is controlled by energy landscape roughness. *J Chem Phys* 131:195101.
31. Jäger M, Nguyen H, Crane JC, Kelly JW, Gruebele M (2001) The folding mechanism of a beta-sheet: The WW domain. *J Mol Biol* 311:373–393.
32. Ferguson N, Johnson CM, Macias M, Oschkinat H, Fersht A (2001) Ultrafast folding of WW domains without structured aromatic clusters in the denatured state. *Proc Natl Acad Sci USA* 98:13002–13007.
33. Liu F, et al. (2008) An experimental survey of the transition between two-state and downhill protein folding scenarios. *Proc Natl Acad Sci USA* 105:2369–2374.
34. Piana S, et al. (2011) Computational design and experimental testing of the fastest-folding β-sheet protein. *J Mol Biol* 405:43–48.
35. Iglesias-Bexiga M, et al. (2018) Protein folding cooperativity and thermodynamic barriers of the simplest beta-sheet fold: A survey of WW domains. *J Phys Chem B* 122:11058–11071.
36. Muñoz V, Campos LA, Sadqi M (2016) Limited cooperativity in protein folding. *Curr Opin Struct Biol* 36:58–66.
37. Sadqi M, Lapidus LJ, Muñoz V (2003) How fast is protein hydrophobic collapse? *Proc Natl Acad Sci USA* 100:12117–12122.
38. Freddolino PL, Liu F, Gruebele M, Schulten K (2008) Ten-microsecond molecular dynamics simulation of a fast-folding WW domain. *Biophys J* 94:L75–L77.
39. Muñoz V (2007) Conformational dynamics and ensembles in protein folding. *Annu Rev Biophys Biomol Struct* 36:395–412.
40. Naganathan AN, Doshi U, Muñoz V (2007) Protein folding kinetics: Barrier effects in chemical and thermal denaturation experiments. *J Am Chem Soc* 129:5673–5682.
41. De Sancho D, Doshi U, Muñoz V (2009) Protein folding rates and stability: How much is there beyond size? *J Am Chem Soc* 131:2074–2075.
42. Borgia A, et al. (2012) Localizing internal friction along the reaction coordinate of protein folding by combining ensemble and single-molecule fluorescence spectroscopy. *Nat Commun* 3:1195.
43. Liu J, et al. (2012) Exploring one-state downhill protein folding in single molecules. *Proc Natl Acad Sci USA* 109:179–184.
44. Roder H, Colón W (1997) Kinetic role of early intermediates in protein folding. *Curr Opin Struct Biol* 7:15–28.
45. Naganathan AN, Li P, Perez-Jimenez R, Sanchez-Ruiz JM, Muñoz V (2010) Navigating the downhill protein folding regime via structural homologues. *J Am Chem Soc* 132:11183–11190.
46. Fung A, Li P, Godoy-Ruiz R, Sanchez-Ruiz JM, Muñoz V (2008) Expanding the realm of ultrafast protein folding: gpW, a midsize natural single-domain with alpha+beta topology that folds downhill. *J Am Chem Soc* 130:7489–7495.
47. Muñoz V, Thompson PA, Hofrichter J, Eaton WA (1997) Folding dynamics and mechanism of beta-hairpin formation. *Nature* 390:196–199.
48. Hagen SJ (2010) Solvent viscosity and friction in protein folding dynamics. *Curr Protein Pept Sci* 11:385–395.
49. Sadqi M, de Alba E, Pérez-Jiménez R, Sanchez-Ruiz JM, Muñoz V (2009) A designed protein as experimental model of primordial folding. *Proc Natl Acad Sci USA* 106:4127–4132.
50. Sanchez-Medina C, et al. (2014) Probing the free energy landscape of the fast-folding gpW protein by relaxation dispersion NMR. *J Am Chem Soc* 136:7444–7451.